DOI: 10.13009/EUCASS2025-481
11TH EUROPEAN CONFERENCE FOR AERONAUTICS AND SPACE SCIENCES (EUCASS)

Numerical investigation of transcritical and doubly-transcritical oxygen-methane flames

Davide Cavalieri[⋆†], *Davide Schintu* [⋆], *Pietro Paolo Ciottoli* [⋆],
Pasquale Eduardo Lapenna[⋆], Francesco Creta [⋆]
[⋆]*Department of Mechanical and Aerospace Engineering, Sapienza University of Rome, Italy*
Via Eudossiana 18
[†]Corresponding author: Davide Cavalieri, davide.cavalieri@uniroma1.it

Abstract

This work presents a computational fluid dynamics framework for simulating transcritical and doubly transcritical oxygen-methane flames, incorporating multicomponent real-fluid thermodynamics and vapor-liquid equilibrium (VLE) modeling. Phase instability is assessed using the tangent plane distance (TPD) method. Results show that in transcritical conditions, phase separation is localized near the LOx core with limited impact on the flow. In doubly-transcritical conditions, unstable regions are more widespread, including both oxidizer and fuel sides. This is linked to the combination of heavier species accumulation and lower local temperatures, promoting the formation of extended regions prone to phase separation.

1. Introduction

Liquid-propellant rocket engines (LREs) operate under extreme thermodynamic conditions, where combustion chamber pressures often exceed the critical pressure of the propellants. Injected at cryogenic temperatures, the oxidizer and/or fuel undergo a pseudo-phase transition from a dense liquid-like state to a gas-like state, experiencing transcritical conditions.[15] These transcritical injection processes exhibit pronounced real-fluid effects, resulting in thermodynamic nonlinearities. Among the various phenomena involved, particular attention has been devoted to the complex interplay between thermodynamic nonlinearities, primarily governed by the pseudo-boiling mechanism,[1] and the turbulent flow dynamics that control injection, mixing, and combustion under LRE conditions.

In recent decades, significant research efforts have been dedicated to understanding these processes at supercritical pressures, both experimentally[4,24–26,32,33,41] and numerically.[2,8,19–21,29,30,36,39,44] These studies have consistently highlighted the crucial role of fluid thermophysical properties in governing thermal jet breakup. As the injected fluid crosses the specific heat peak, an extended liquid core can form, underlining the importance of real-fluid effects during liquid-like injection conditions. The near-critical enhancement of thermodynamic and transport properties has a significant influence on combustion dynamics and flame structure. In particular, under transcritical conditions, heat and mass transfer between the dense liquid core and the surrounding gas phase are primarily controlled by turbulent mixing, with pseudo-vaporization of the cryogenic propellants emerging as the rate-limiting mechanism.

Recently, increasing attention has been devoted to the possibility of phase-separation phenomena driven by the elevation of the mixture critical point in multicomponent systems. While absent in pure fluids, these effects can arise when composition variations shift the local critical point above that of the pure components, potentially inducing two-phase behavior even at nominally supercritical pressures. Experimental studies have provided evidence of such phenomena in both LRE conditions[23] and for hydrocarbon-nitrogen mixtures.[10,43]

In parallel, computational fluid dynamics (CFD) simulations have attempted to characterize these phase-separation effects. An alternative modeling strategy gaining relevance relies on thermodynamic frameworks rooted in vapor-liquid equilibrium (VLE) principles. Within this approach, the mixture is described by explicitly resolving the coexistence of vapor and liquid phases through the introduction of a phase fraction parameter. This parameter governs the local partitioning between the two phases, enabling a continuous treatment of both homogeneous supercritical states and heterogeneous two-phase regimes, allowing the capture of the onset of thermodynamic instabilities.

For inert mixing, several studies have investigated the effects of multicomponent phase-separation on mixing characteristics and injection dynamics.[3,5,22,37,45] Only a few of them addressed LRE propellant combinations.[3,5] For reacting flows, Traxiger et al.,[44] coupled VLE thermodynamics with a flamelet-based Large-Eddy simulations (LES) approach to simulate transcritical oxygen-methane flames, identifying the LOx core, where pure oxygen interacts with combustion products, as the primary region of phase separation. Recently, Tudisco and Menon[46] investigated CH_4/O_2

Copyright © 2025 by D. Cavalieri. Published by the EUCASS association with permission.

DOI: 10.13009/EUCASS2025-481

mixing and combustion in a canonical temporal-mixing-layer configuration, using a five-species kinetic scheme with a state-of-the-art VLE modeling. Their results showed only minor differences between VLE and non-VLE solutions in the reacting case. Near the flame, VLE states formed primarily on the vapor side, with small amounts of H_2O driving phase separation, while CO and CO_2 played a secondary role.

Given these considerations, this contribution employs a real-fluid VLE flamelet-based methodology to investigate the onset of the phase-separation phenomenon for an oxygen-methane flame under transcritical (LOx-GCH_4) conditions, and extends the analysis to a doubly transcritical (LOx-LCH_4) case. First, we analyze the impact of VLE thermodynamics on a LOx-LCH_4 laminar flame structure, delineating the thermodynamically unstable state in an a-priori fashion. Then, leveraging the LES approach, two-phase effects are addressed and their impact discussed.

2. Methods

2.1 Thermodynamic and combustion modeling

At cryogenic and supercritical conditions, the ideal gas law fails to accurately describe the coupling between pressure, density, and temperature. Accurate numerical modeling of such processes requires the adoption of appropriate thermodynamic closure relations. In this context, cubic equations of state (EoS) are commonly employed in CFD simulations of transcritical flows. These models incorporate key physical phenomena, including intermolecular attractive forces a and the finite molecular co-volume b. In the present work, the Soave-Redlich-Kwong (SRK) EoS[42] is adopted to model the thermodynamic behavior of such fluids as:

$$p(T,\rho) = \frac{\rho \mathcal{R} T}{M - b\rho} - \frac{a\alpha(T)\rho^2}{M^2 + 2Mb\rho}, \tag{1}$$

where p is the pressure, $\mathcal{R}$ is the universal gas constant, ρ is the density of the mixture, T is the temperature and M is the molar mass. To extend the SRK-EoS to multicomponent mixtures, the single-fluid assumption along with conventional mixing rules[17,35] are used to evaluate the EoS parameters:

$$a = \sum_{k=1}^{N_s}\sum_{j=1}^{N_s} X_k X_j a_{kj}; \qquad b = \sum_{k=1}^{N_s} X_k b_k \tag{2}$$

where N_s is the number of species, X are the species molar fractions, while the single-component EoS non-ideal parameters (a_k and b_k) can be found in the original work.[42] The departure function formalism [35] is used to compute the caloric properties, while the molecular viscosity μ, and the thermal conductivity k, are calculated using the semi-empirical Chung's[9] model.

As previously introduced, during mixing and combustion, regions may experience local subcritical conditions, which can trigger phase separation. Accurately predicting the thermophysical behavior of the mixture under these circumstances requires a specific thermodynamic approach. To handle this, the SRK-EoS has been coupled with a two-phase modeling framework that applies the VLE criteria. For a generic mixture characterized by its thermodynamic state (T, p, X), equilibrium is achieved when mechanical, thermal, and chemical balances are simultaneously satisfied. Under these conditions, the system fulfills the vapor-liquid equilibrium (VLE) condition:[12]

$$p^L = p^V = p; \quad T^L = T^V = T; \quad f_i^L = f_i^V \quad i = 1, ..., N_s \tag{3}$$

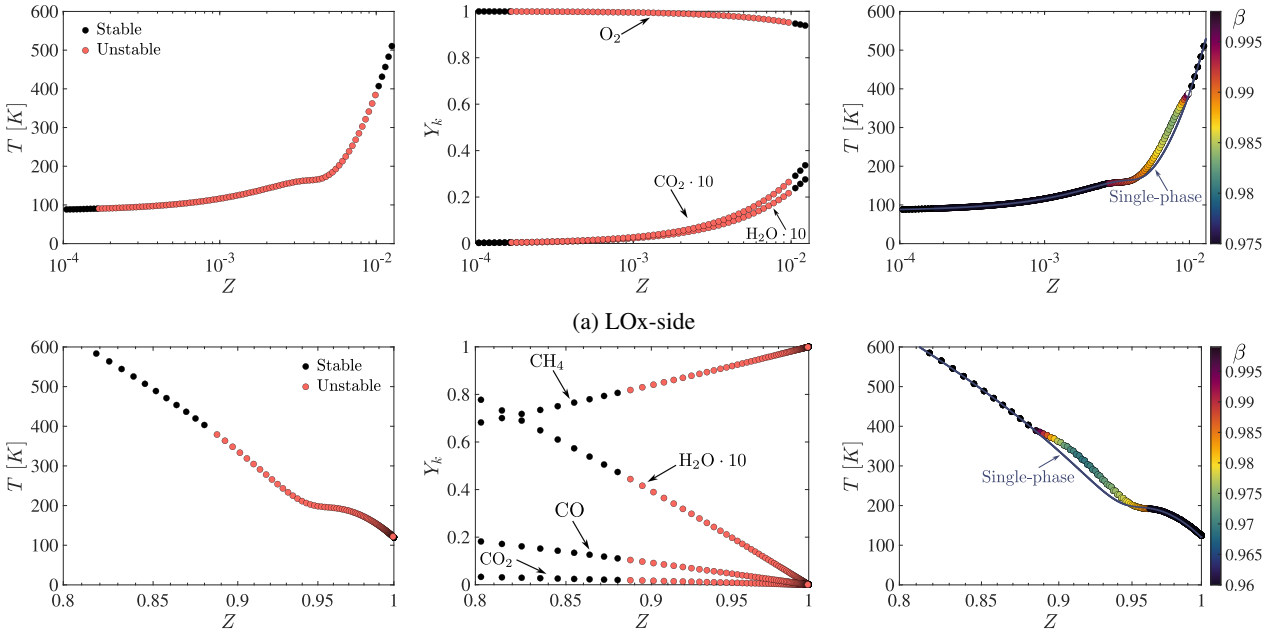
where f_i is the fugacity of component i, the superscript V and L refer to the vapor and liquid phases, respectively. The fugacity of component i can be derived analytically given the selected EoS.[12,27] Besides chemical equilibrium, mass conservation must also be satisfied for each species i, relating the mole fractions in the liquid (x_i) and vapor (y_i) phases to the overall composition (X_i).[12,27] The combination of mass balance constraints and Gibbs energy minimization, enforced via fugacity equality, results in a nonlinear system of equations defined by the thermodynamic state (T, p, X) with the unknowns (β, x_i, y_i), where β represents the vapor phase fraction, i.e., the ratio between the number of moles in the vapor phase and the total moles in the system. This formulation corresponds to the classical isothermal-isobaric flash problem, consisting of $N_s + 1$ nonlinear equations.[12,27] Details regarding the algorithm, the practical implementation to solve the isothermal-isobaric flash problem, and its validation can be found in the authors' previous work.[5,7] After determining the vapor fraction and the phase compositions, the bulk properties of the mixture at phase equilibrium can be evaluated using appropriate mixing rules, the generic thermodynamic property ψ is obtained according to

$$\psi^{VLE}(T, p, X) = \beta\psi^V(T, p, y) + (1 - \beta)\psi^L(T, p, x). \tag{4}$$

DOI: 10.13009/EUCASS2025-481

Finally, the combustion model is based on the flamelet approach.[34] In this framework, the complex structure of a turbulent non-premixed flame is represented as a collection of laminar flames, each defined in the mixture fraction space Z. In particular, the thermodynamic manifold is obtained by solving the flamelet equation with the phase-equilibrium thermodynamics described previously.

In this regard, Fig. 1 reports a detailed analysis, considering phase-separation, of an oxygen-methane flame at doubly-transcritical conditions, i.e., $p = 56bar$, oxidizer $T_{O_2} = 85\ K$, and fuel inlet temperature $T_{CH_4} = 120\ K$, respectively. Specifically, to identify where phase instability occurs across the mixture fraction space and to characterize the thermodynamic state in terms of temperature and species composition, we apply the tangent plane distance (TPD) method of Michelsen.[28] Red dots indicate unstable thermodynamic states, while black dots correspond to stable conditions, based on the TPD analysis. On the LOx-rich side (Fig. 1a), phase instability emerges at very low mixture fractions ($Z < 10^{-2}$). This behavior is triggered by the presence of small yet non-negligible amounts of combustion products, particularly CO_2 and H_2O, in a predominantly oxidizer environment. Although these species are present in trace amounts, their non-ideal interactions with O_2 significantly affect the local thermodynamic stability. Moreover, consistently with what was observed in,[44] the phase fraction β is closed to unity ($0.97 < \beta < 0.995$), and using a VLE modeling results in a higher temperature prediction when a two-phase state occurs. On the fuel-rich side (Fig. 1b), phase instability occurs in the range $0.87 < Z < 0.97$. Here, the presence of carbon-based species such as CO, and CO_2 is not present in trace amounts. As a result, more appreciable differences appear between the stable and unstable branches in the temperature profile.



(a) LOx-side

(b) LCH_4 side

Figure 1: Laminar oxygen-methane flame structure analysis at supercritical pressure ($p = 56\ bar$) for: (a) LOx-side and (b) LCH_4-side.

2.2 Governing equations

The thermodynamic modeling reported in the following sections is a part of a numerical framework that solves the Favre-filtered conservation equations in terms of mass and momentum

$$\frac{\partial \overline{\rho}}{\partial t} + \frac{\partial \overline{\rho}\tilde{u}_j}{\partial x_j} = 0, \tag{5}$$

$$\frac{\partial \overline{\rho}\tilde{u}_i}{\partial t} + \frac{\partial \overline{\rho}\tilde{u}_i\tilde{u}_j}{\partial x_j} = -\frac{\partial \overline{p}_1}{\partial x_i} + \frac{\partial \overline{\tau}_{ij}}{\partial x_j} + \frac{\partial \tau_{ij}^{sgs}}{\partial x_j}, \tag{6}$$

where $\overline{\bullet}$ and $\tilde{\bullet}$ respectively denote the spatial filtering and the Favre-filtering operation, i.e., $\tilde{\bullet} = \overline{\rho\bullet}/\overline{\rho}$, while u_i are the velocity components. The fluid mixture is assumed to be Newtonian, with the resolved and modeled viscous stress tensors written as

DOI: 10.13009/EUCASS2025-481

$$\overline{\tau}_{ij} + \tau_{ij}^{sgs} = 2\left(\overline{\mu} + \overline{\rho}\nu^{sgs}\right)\left(\tilde{S}_{ij} - \frac{1}{3}\delta_{ij}\tilde{S}_{kk}\right), \tag{7}$$

where S_{ij} is the strain rate tensor, and δ_{ij} is the Kronecker-Delta. The SGS kinematic viscosity ν^{sgs} is modeled using the WALE model.[31] In flamelet-based LES, two additional transport equations are solved for the filtered mixture fraction and its variance to describe the turbulent flame with the look-up process of the flamelet libraries.[16] These equations read:

$$\frac{\partial\overline{\rho}\tilde{Z}}{\partial t} + \frac{\partial\overline{\rho}\tilde{u}_j\tilde{Z}}{\partial x_j} = \frac{\partial}{\partial x_j}\left[\left(\overline{\mathcal{D}} + \mathcal{D}^{sgs}\right)\frac{\partial\tilde{Z}}{\partial x_j}\right], \tag{8}$$

$$\frac{\partial\overline{\rho}\widetilde{Z''^2}}{\partial t} + \frac{\partial\overline{\rho}\tilde{u}_j\widetilde{Z''^2}}{\partial x_j} = \frac{\partial}{\partial x_j}\left[\left(\overline{\mathcal{D}} + \mathcal{D}^{sgs}\right)\frac{\partial\widetilde{Z''^2}}{\partial x_j}\right] - 2\overline{\rho}\tilde{\chi} + 2\left(\overline{\mathcal{D}} + \mathcal{D}^{sgs}\right)\left(\frac{\partial\tilde{Z}}{\partial x_j}\right)^2, \tag{9}$$

where $\overline{\mathcal{D}} = \overline{(\lambda/c_p)}$ and $\mathcal{D}^{sgs} = \overline{\rho}\nu^{sgs}/Sc_t$ are the molecular and sub-grid diffusivity, respectively. The turbulent Schmidt number is $Sc_t = 0.7$ in all simulations. Following,[11] the scalar dissipation rate $\tilde{\chi}$ is modeled decomposing it into resolved and SGS term as

$$2\overline{\rho}\tilde{\chi} = 2\overline{\mathcal{D}}\left(\frac{\partial\tilde{Z}}{\partial x_j}\right)^2 + C_\chi\mathcal{D}^{sgs}\frac{\widetilde{Z''^2}}{\Delta}, \tag{10}$$

where C_χ is a model constant set to 2, and Δ denotes the local filter size computed as the cube root of the cell volume.

3. Test case and numerical setup

To analyze the impact of phase separation phenomena in liquid-propellant rocket engines under transcritical and doubly transcritical injection conditions, the Mascotte experimental test case, as described by Singla et al.,[41] is adapted as a reference. Specifically, in the transcritical LOx-GCH_4 flame (TF) configuration, the chamber pressure is set to 56.1 bar, which exceeds the critical pressures of both oxidizer and fuel. Liquid oxygen is injected in a liquid-like state at $T = 85$ K, while methane is injected in a supercritical state at $T = 288$ K. Under these operating conditions, the corresponding fluid densities are $\rho_{O_2} = 1180$ kg/m^3 for oxygen and $\rho_{CH_4} = 42$ kg/m^3 for methane. The propellant mass flow rates are $\dot{m}_{O_2} = 44.4$ g/s and $\dot{m}_{CH_4} = 143.1$ g/s, resulting in a global mixture ratio of $E = \dot{m}_{O_2}/\dot{m}_{CH_4} = 0.31$. This test case has been extensively investigated in the literature and is widely recognized as a benchmark for validating numerical solvers[39] and turbulent combustion models[21,49] under LRE-relevant conditions. In addition, Traxinger et al.[44] used the same test case to study the two-phase phenomena in transcritical flow under LRE relevant conditions. For the injector configuration adopted in this work, the geometric parameters have been selected based on the specifications reported in previous studies.[18,21,40,47] Lastly, a LOx-LCH_4 doubly transcritical flame (DTF) configuration is considered. The chamber pressure, propellant mass flow rates, and liquid oxygen injection temperature are maintained identical to those of the TF case. To establish doubly transcritical conditions, the methane injection temperature is reduced to $T = 120$ K, placing it in a liquid-like thermodynamic state with a corresponding density of 414 kg/m^3. The injector geometry for the DTF case retains the same inner oxygen post diameter and post-tip width as in the TF configuration. To preserve comparable injection dynamics, the methane injector annulus height is adjusted to match the momentum flux ratio of the TF case. The complete set of operating, injector parameters, and computational domain details, for both configurations, can be found in.[8]

Regarding the numerical setup, the LES were performed using an in-house finite-volume solver with tabulated chemistry capabilities, developed within the OpenFOAM framework.[48] This computational platform has been extensively applied to high-pressure reacting and non-reacting flows under LRE-relevant conditions in previous LES studies.[8,13,14,38] Its predictive capabilities were recently validated for highly stratified transcritical conditions,[5,6] as encountered in the present study. Moreover, diffusive and convective fluxes are estimated using a second-order accurate centered difference scheme. Temporal integration is performed using the implicit Euler scheme, with a maximum Courant-Friedrichs-Lewy condition of CFL = 0.4. To limit computational demand, the axial length of the domain is set to 200 mm, which tests have confirmed to be sufficient to prevent recirculation and avoid flame-outlet interactions. The walls are treated as adiabatic with standard wall-law conditions, while a fixed pressure (Dirichlet) condition is imposed at the outlet. The simulations were performed using an O-type hexahedral grid containing approximately 13.1 million finite volumes. The finest cells, at the injector lip measure 100 μm. Downstream, the grid is progressively coarsened with an axial expansion ratio below 1.003. Details regarding the grid sensitivity analysis for the same test case can be found in.[8]

DOI: 10.13009/EUCASS2025-481

4. Results and discussion

In this section, we provide a qualitative analysis of the phase-separation effects obtained for both investigated configurations. Instantaneous fields extracted along a longitudinal cut of the computational domain are shown in the following figures.

As a first step, the regions affected by phase separation are identified through the thermodynamic stability sensor, displayed in Figure 2. The sensor is computed using the TPD method, which assesses the local thermodynamic stability of the mixture. In the figure, blue areas correspond to stable, single-phase regions, while red areas highlight zones where the mixture becomes thermodynamically unstable and phase-separation occurs. In the transcritical case, phase separation is primarily restricted to the LOx core, where the dense, cold oxidizer interacts with the surrounding combustion products. The unstable region remains relatively localized and limited to the near-field of the oxidizer jet. In contrast, the doubly-transcritical configuration-which involves the injection of both oxidizer and fuel under cryogenic conditions-exhibits a markedly broader and more fragmented unstable region. Notably, unstable region also occurs on the annular fuel side, where cryogenic methane interacts with the hotter recirculating gases and the flame. For both streams, large scale pocket of unstable mixtures detach and disappear as they mixes and burns with the surrounding gases.

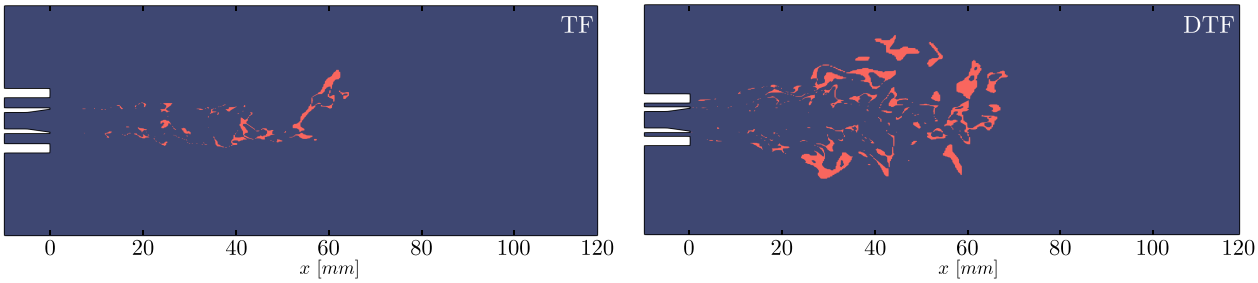


Figure 2: Instantaneous field of the stability sensor (blue: stable, red: unstable) of the transcritical (left-panel) and doubly-transcritical (right-panel) flames.

To provide a quantitative measure of phase separation, Figure 3 presents instantaneous fields of the vapor phase fraction $\tilde{\beta}$ superimposed on the mixture fraction $\tilde{Z}$. In the transcritical configuration, a narrow zone of phase separation develops along the flame front, consistent with the trends observed in Fig.2 and previously reported in.[44,46] The vapor phase fraction remains predominantly close to unity, indicating that only limited portions of the mixture undergo phase instability, with a minor amount of liquid condensation near the high-temperature shear layers where pure oxygen mixes with water and carbon dioxide (see Fig. 1). In contrast, the doubly-transcritical flame exhibits a markedly different behavior. The phase separation extends more broadly, with significant two-phase regions appearing both along the oxidizer core and in the methane annular jet. As a result, the vapor phase fraction field reveals multiple fragmented pockets with $\tilde{\beta}$ values substantially lower than unity, indicating the formation of larger amounts of condensed phase. The increased spatial extent of phase separation observed in the DTF case suggests a stronger thermodynamic coupling between multicomponent phase behavior, turbulent mixing, and flame stabilization mechanisms.

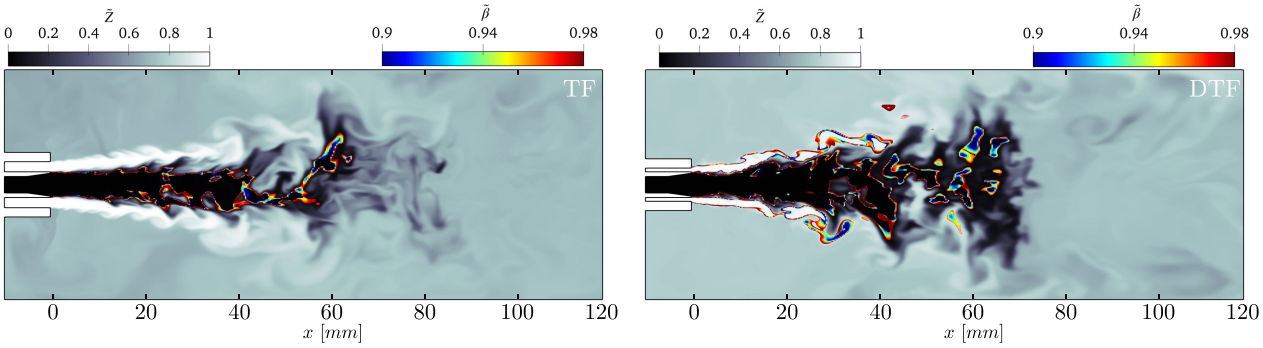


Figure 3: Phase-separation effects comparison between transcritical (left-panel) and doubly-transcritical (right-panel) flames. Longitudinal slice of the vapor phase fraction field superimposed on the mixture fraction.

To further quantify the statistical characteristics of phase separation, Figure 4 reports the joint probability density function (JPDF) of the vapor phase fraction $\tilde{\beta}$ and mixture fraction $\tilde{Z}$ for both configurations. In the transcritical case

DOI: 10.13009/EUCASS2025-481

(left panel), the JPDF is strongly concentrated near $\tilde{\beta} \approx 1$, confirming that the majority of the flow remains in a stable single-phase regime. Only a small portion of the samples exhibits vapor phase fractions slightly below unity, and these occur primarily at low $\tilde{Z}$ values, corresponding to oxidizer-rich mixtures close to the LOx core, where localized condensation may occur.

The DTF configuration exhibits a markedly different statistical behavior. The JPDF shows a broader spread of $\tilde{\beta}$ values, especially towards lower $\tilde{\beta}$ at high $\tilde{Z}$ values, i.e., in fuel-rich regions. Despite the fact that methane is injected at a higher initial temperature compared to oxygen, the normalized PDF reveals a higher probability of multiphase events on the fuel-rich side. This can be attributed to two main effects: first, the presence of multiple heavy species and combustion intermediates on the fuel side alters the mixture composition, increasing the non-idealities and reducing the stability margins of the phase envelope. Second, the fuel-rich mixing layer tends to develop a relatively colder thermal plateau, resulting from the strong thermal inertia of the dense cryogenic methane (see[8] for additional details), which limits the temperature rise despite mixing with hot products. The combination of heavier species accumulation and lower local temperatures promotes the formation of extended regions prone to phase separation on the fuel-rich side, even though the initial injection condition of the fuel is relatively less cryogenic than the oxidizer.

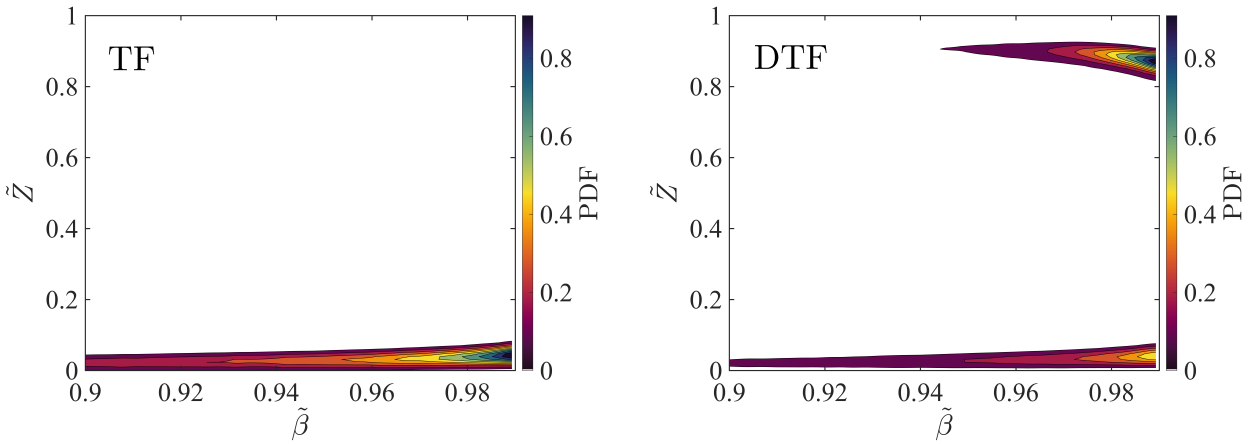


Figure 4: Statistical features of the phase-separation. Joint probability density function between $\tilde{\beta}$ and $\tilde{Z}$, for (a) TF (b) DTF.

5. Conclusions

This work presented a computational framework for the simulation of transcritical and doubly-transcritical flames, incorporating multicomponent real-fluid thermodynamics and vapor-liquid equilibrium modeling. The framework is based on the SRK cubic equation of state, extended to handle phase separation phenomena. A detailed analysis has been conducted to assess the impact of phase separation under different thermodynamic conditions. Using the TPD method, the presence of unstable thermodynamic regions has been detected in both transcritical and doubly-transcritical configurations. For the transcritical flame, phase separation is confined to localized areas, primarily near the LOx jet core, where oxygen mixes with water vapor and carbon dioxide. The effect on the overall flow field is limited, and the vapor phase fraction remains close to unity across most of the domain. In contrast, the doubly-transcritical configuration shows a much broader and more fragmented distribution of unstable regions. Phase separation occurs both on the oxidizer side and, significantly, in the annular methane jet. This is attributed to the combination of local thermal stratification and species accumulation, which lowers the phase stability margin even though the methane is injected at a higher temperature than oxygen. Joint PDF analyses confirmed the higher likelihood of multiphase conditions on the fuel-rich side. Future work will focus on extending the current analysis to different pressure regimes. Particular attention will be given to quantifying the influence of phase separation on flame stabilization, ignition behavior, and heat transfer.

6. Acknowledgments

The authors acknowledge the support of the Italian Ministry of University and Research (MUR). D. Cavalieri acknowledges the support of the project: "Advanced Numerical Modeling of Thermodynamics and Thermochemistry in Green

DOI: 10.13009/EUCASS2025-481

Aerospace Engines", funded by PON RI 2014-2020, as well as the Young Researcher and Innovator Conference Grant: E-COST-GRANT-CA22151-bedaa535.

References

[1] D.T. Banuti. Crossing the Widom-line-Supercritical pseudo-boiling. *Jour. Supercrit. Fluids*, 98:12–16, 2015.

[2] D.T. Banuti, P.C. Ma, J.P. Hickey, and M. Ihme. Thermodynamic structure of supercritical LOX-GH2 diffusion flames. *Combust. Flame*, 196:364–376, 2018.

[3] D.T. Banuti, P.C. Ma, and M. Ihme. *Phase separation analysis in supercritical injection using large-eddy-simulation and vapor-liquid-equilibrium*. 53rd AIAA/SAE/ASEE Joint Propulsion Conference, 2017.

[4] S. Candel, M. Juniper, G. Singla, P. Scouflaire, and C. Rolon. Structure and dynamics of cryogenic flames at supercritical pressure. *Combust. Sci. Technol*, 178(1-3):161–192, 2006.

[5] D. Cavalieri, G. Indelicato, A. Remiddi, F. Creta, P.P. Ciottoli, and P.E. Lapenna. Assessment of phase-separation phenomena in LREs cryogenic flows. In *Aerospace Europe Conference 2023 - 10th EUCASS- 9th CEAS*, 2023.

[6] D. Cavalieri, G. Indelicato, A. Remiddi, F. Creta, and P.P. Ciottoli P.E. Lapenna. A pressure-based numerical framework for highly stratified transcritical real-fluids simulations. In *AIAA SCITECH 2023 Forum*, 2023.

[7] D. Cavalieri, J. Liberatori, M. Blandino, P.E. Lapenna, M. Valorani, and P.P. Ciottoli. Evaluation of Non-ideal Fluid Modeling for Droplet Evaporation in Jet-Engine-Like Conditions. *Flow Turbul. Combust.*, 114:857–885, 2025.

[8] D. Cavalieri, D. Schintu, P.P. Ciottoli, P.E. Lapenna, and F. Creta. Characterization of turbulent pseudo-boiling in transcritical and doubly-transcritical oxygen-methane flames. *Int. Jour. Heat and Mass Transfer*, 251:127284, 2025.

[9] T.H. Chung, M. Ajlan, L.L. Lee, and K.E. Starling. Generalized multiparameter correlation for nonpolar and polar fluid transport properties. *Ind. & Eng. Chem. Res.*, 27(4):671–679, 1988.

[10] C. Crua, J. Manin, and L. M. Pickett. On the transcritical mixing of fuels at diesel engine conditions. *Fuel*, 208:535–548, 2017.

[11] P. Domingo, L. Vervisch, and D. Veynante. Large-eddy simulation of a lifted methane jet flame in a vitiated coflow. *Combust. Flame*, 152(3):415–432, 2008.

[12] J. R. Elliott and C. T. Lira. *Introductory chemical engineering thermodynamics*. Prentice Hall PTR, Upper Saddle River, NJ, 1999.

[13] G. Indelicato and F. Creta. Assessment of an algebraic equilibrium wall-function for supercritical flows. *Int. Jour. Heat Mass Transf.*, 197:123350, 2022.

[14] G. Indelicato, A. Remiddi, P.E. Lapenna, F. Creta, N.P. Longmire, and D.T. Banuti. Dataset of Wall-Resolved Large-Eddy Simulations Turbulent Pseudoboiling in Cryogenic Hydrogen Pipe Flows. *Jour. Thermophys. Heat Transf.*, 37(1):133–146, 2023.

[15] L. Jofre and J. Urzay. Transcritical diffuse-interface hydrodynamics of propellants in high-pressure combustors of chemical propulsion systems. *Prog. Energy Combust. Sci.*, 82:100877, 2021.

[16] K.A. Kemenov, H. Wang, and S.B. Pope. Modelling effects of subgrid-scale mixture fraction variance in les of a piloted diffusion flame. *Combust. Theory Model.*, 16(4):611–638, 2012.

[17] S.K. Kim, H.S. Choi, and Y. Kim. Thermodynamic modeling based on a generalized cubic equation of state for kerosene/LOx rocket combustion. *Combust. Flame*, 159(3):1351–1365, 2012.

[18] T. Kim, Y. Kim, and S.K. Kim. Effects of pressure and inlet temperature on coaxial gaseous methane/liquid oxygen turbulent jet flame under transcritical conditions. *Jour. Supercrit. Fluids*, 81:164–174, 2013.

[19] P.E. Lapenna. Characterization of pseudo-boiling in a transcritical nitrogen jet. *Phys. Fluids*, 30(7):077106, 2018.

DOI: 10.13009/EUCASS2025-481

[20] P.E. Lapenna, P.P. Ciottoli, and F. Creta. Unsteady Non-Premixed Methane/Oxygen Flame Structures at Supercritical Pressures. *Combust. Sci. Technol*, 189(12):2056–2082, 2017.

[21] P.E. Lapenna, G. Indelicato, R. Lamioni, and F. Creta. Modeling the equations of state using a flamelet approach in LRE-like conditions. *Acta Astronaut.*, 158:460–469, 2019.

[22] J. Matheis and S. Hickel. Multi-component vapor-liquid equilibrium model for les of high-pressure fuel injection and application to ECN Spray-A. *Int. Jour. of Multiphase Flow*, 99:294–311, 2018.

[23] W. Mayer, A. Schik, M. Schaffler, and H. Tamura. Injection and mixing processes in high-pressure liquid oxygen/gaseous hydrogen rocket combustors. *Jour. of Prop. and Power*, 16(5):823–828, 2000.

[24] W. Mayer and H. Tamura. Propellant injection in a liquid oxygen/gaseous hydrogen rocket engine. *Jour. Propul. Power*, 12:1137–1147, 1996.

[25] W. Mayer, J. Telaar, R. Branam, G. Schneider, and J. Hussong. Raman Measurements of Cryogenic Injection at Supercritical Pressure. *Heat Mass Transf.*, 39:709–719, 2003.

[26] W.O.H. Mayer, A.H.A Schik, B. Vielle, C. Chauveau, I. Gokalp, D.G. Talley, and R.D. Woodward. Atomization and Breakup of Cryogenic Propellants Under High-Pressure Subcritical and Supercritical Conditions. *Jour. Propul. Power*, 14(5):835–842, 1998.

[27] Michael Locht Michelsen and Jørgen Mollerup. *Thermodynamic Modelling: Fundamentals and Computational Aspects*. Tie-Line Publications, 2004.

[28] M.L. Michelsen. The isothermal flash problem. part i. stability. *Fluid Phase Equilibria*, 9(1):1–19, 1982.

[29] F. Monnier and G. Ribert. Numerical simulations of supercritical CH4/O2 flame propagation in inhomogeneous mixtures following ignition. *Proc. Combust. Inst.*, 39(2):2747–2755, 2023.

[30] F. Monnier, G. Ribert, and L. D. Duvilla. CH4/O2 supercritical flame structure and simulation. *Proc. Combust. Inst.*, 40(1):105514, 2024.

[31] F. Nicoud and F. Ducros. Subgrid-Scale Stress Modelling Based on the Square of the Velocity Gradient Tensor. *Flow Turbul. Combust.*, 62:183–200, 1999.

[32] M. Oschwald and A. Schik. Supercritical nitrogen free jet investigated by spontaneous Raman scattering. *Exp. Fluids*, 27:497–506, 1999.

[33] M. Oschwald, J.J. Smith, R. Branam, J. Hussong, A. Schik, B. Chehroudi, and D. Talley. Injection of fluids into supercritical environments. *Combust. Sci. Technol*, 178(1-3):49–100, 2006.

[34] N. Peters. Laminar flamelet concepts in turbulent combustion. *Twenty-First Symposium (International) on Combustion*, 21(1):1231–1250, 1988.

[35] B.E. Poiling, J.M. Prausnitz, and J.P. O'Connel. *The properties of gases and liquids*. McGraw-Hill Education, 5th edition, 2001.

[36] L. Pons, N. Darabiha, G. Ribert S. Candel, and V. Yang. Mass transfer and combustion in transcritical nonpremixed counterflows. *Combust. Theory Model.*, 13(1):57–81, 2009.

[37] L. Qiu and R.D. Reitz. An investigation of thermodynamic states during high-pressure fuel injection using equilibrium thermodynamics. *Int. Jour. Multiphase Flow*, 72:24–38, 2015.

[38] D. Schintu, D. Cavalieri, A. Remiddi, G. Indelicato, F. Creta, and P.E. Lapenna. Efficient multiphysics simulations of lre combustion chambers using tabulated chemistry. In *Proceedings of the 9th Edition of the 3AF International Space Propulsion Conference*, 2024.

[39] T. Schmitt. Large-Eddy Simulations of the Mascotte Test Cases Operating at Supercritical Pressure. *Flow Turbul. Combust.*, 105(1):159â189, 2020.

[40] A. Sharma, A. De, and S.S. Kumar. Numerical investigation of supercritical combustion dynamics in a multi-element LOx-methane combustor using flamelet-generated manifold approach. *Phys. Fluids*, 35(11):115125, 2023.

DOI: 10.13009/EUCASS2025-481

[41] G. Singla, P. Scouflaire, C. Rolon, and S. Candel. Transcritical oxygen/transcritical or supercritical methane combustion. *Proc. Combust. Inst.*, 30(2):2921–2928, 2005.

[42] G. Soave. Equilibrium constants from a modified Redlich-Kwong equation of state. *Chem. Eng. Sci.*, 27(6):1197–1203, 1972.

[43] C. Traxinger, M. Pfitzner, S. Baab, G. Lamanna, and B. Weigand. Experimental and numerical investigation of phase separation due to multicomponent mixing at high-pressure conditions. *Phys. Rev. Fluids*, 4:074303, Jul 2019.

[44] C. Traxinger, J. Zips, and M. Pfitzner. Single-Phase Instability in Non-Premixed Flames under Liquid Rocket Engine Relevant Conditions. *J. Propul. Power*, 35(4):675–689, 2019.

[45] P. Tudisco and S. Menon. Numerical investigations of phase-separation during multi-component mixing at supercritical conditions. *Flow Turb. and Combust.*, 104:693–724, 2019.

[46] Principio Tudisco and Suresh Menon. Numerical investigations of thermodynamic states formed near a reacting, supercritical ch4/o2 flame. *Proceedings of the Combustion Institute*, 39(2):2725–2736, 2023.

[47] S. Wang, H. Wang, K. Luo, and J. Fan. The effects of differential diffusion on turbulent non-premixed flames LO2/CH4 under transcritical conditions using large-eddy simulation. *Energies*, 16, 2023.

[48] H.G. Weller, G. Tabor, H. Jasak, and C. Fureby. A tensorial approach to computational continuum mechanics using object-oriented techniques. *Comput. Phys.*, 12(6):620–631, 11 1998.

[49] J. Zips, H. Muller, and M. Pfitzner. Efficient Thermo-Chemistry Tabulation for Non-Premixed Combustion at High-Pressure Conditions. *Flow Turbul. Combust.*, 101:821â850, 2018.